

# ANGULAR UNMIXING OF PHOTOSYNTHETIC AND NON-PHOTOSYNTHETIC VEGETATION WITHIN A CONIFEROUS FOREST USING CHRIS-PROBA

J. Verrelst<sup>a,\*</sup>, R. Zurita-Milla<sup>a</sup>, B. Koetz<sup>b</sup>, J.G.P.W. Clevers<sup>a</sup>, M.E. Schaepman<sup>a</sup>

<sup>a</sup>Centre for Geo-Information, Wageningen UR, Wageningen, The Netherlands – (Jochem.Verrelst, Raul.Zurita-Milla, Jan.Clevers, Michael.Schaepman)@wur.nl

<sup>b</sup>Remote Sensing Laboratories (RSL), Dept. of Geography, University of Zürich, Switzerland – bkoetz@geo.unizh.ch

Commission VII, WG VII/1

**KEY WORDS:** Non-Photosynthetic Vegetation, spectral unmixing, FLIGHT, multiangular, vegetation structure, PV, NPV

## ABSTRACT:

Estimating forest variables, such as photosynthetic light use efficiency, from satellite reflectance data requires understanding the contribution of photosynthetic vegetation (PV) and nonphotosynthetic vegetation (NPV). The fractions of PV and NPV present in vegetation reflectance data are typically controlled by the canopy structure and the respective viewing angle. The persistent but highly varying anisotropic behaviour of the forest canopy implies that there is canopy structural information to be exploited from multi-view angles measurements. In this work, a combination of radiative transfer modelling (FLIGHT) and linear unmixing techniques were used to isolate angular PV and NPV fractions from multi-angular CHRIS-PROBA (Compact High Resolution Imaging Spectrometer-Project for On-board Autonomy) data in order to assess their effects on a suite of vegetation indices. Angular variability in the NIR wavelengths contributed most to the angular change in PV and NPV fractions. In turn, for those pixels where the NPV fractions from near-nadir to backscatter were increasing, moderate correlations were found with the angular variability of the calculated vegetation indices. From these fractions, a Normalized Difference NPV Index (NDNPVI) was developed as a proxy for volumetric canopy composition.

## 1. INTRODUCTION

This study begins with the assumption that pixel level canopy reflectance of a terrestrial ecosystem typically consists of a proportion of Photosynthetic vegetation (PV) and a proportion of Non-Photosynthetic Vegetation (NPV: parts/ canopy components that lack chlorophyll, such as dry leaf matter, bark, wood, and stems) and eventually rock and bare soil. The fractional extent of vegetation into PV and NPV is important from biophysical and biogeochemical perspectives (Defries et al. 1999), as well as to understanding climate and land-use controls (Asner and Heidebrecht 2002). Many approaches have been developed to analyze PV, NPV and bare soil. A problem hereby is that the typical spectral regions used to detect PV – the visible and the NIR wavelengths (0.4-1.3  $\mu\text{m}$ ) - do not easily separate the individual contribution of NPV and bare soil to the measurement (van Leeuwen and Huete 1996, Roberts et al. 1998). Alternatively, spectral mixture analysis was developed to decompose image pixels into its pure constituent (Settle and Drake 1993, Adams et al. 1995). As such, pixel level reflectance can be described by a spectral mixture model in which a mixed spectrum is represented as a linear combination of pure spectra, called endmembers (EMs):

$$R(\lambda)_{\text{pixel}} = f_{\text{PV}}R(\lambda)_{\text{PV}} + f_{\text{NPV}}R(\lambda)_{\text{NPV}} + f_{\text{soil}}R(\lambda)_{\text{soil}}$$

and  $f_{\text{PV}} + f_{\text{NPV}} + f_{\text{soil}} = 1$ , (1)

where  $f_{\text{PV}}$ ,  $f_{\text{NPV}}$ ,  $f_{\text{soil}}$  are the fractions of PV, NPV and soil respectively,  $R(\lambda)$  is the reflectance of each land-cover endmember at wavelength  $\lambda$ . Regarding forested surfaces, it is commonly the case that bare soil or rocks are absent in a pixel but are replaced by understory (e.g. grass or herbaceous

vegetation) or litter cover. Then, a further simplification can be made, namely,

$$R(\lambda)_{\text{pixel}} = f_{\text{PV}}R(\lambda)_{\text{PV}} + (1 - f_{\text{PV}})R(\lambda)_{\text{NPV}} \quad \text{and} \quad 0 \leq f_{\text{PV}} \leq 1. \quad (2)$$

Further, although often ignored in nadir remote sensing, sun/view geometry has a great influence on the observed reflectance of a surface, which is described by its bidirectional reflectance distribution function (BRDF). The magnitude and shape of the BRDF is governed by the composition, density, optical properties and geometric structure of the vegetation canopy. It are these BRDF effects that triggered the current advances in multi-angular remote sensing. Recently numerous studies have demonstrated that measurements from multiple view-angles (e.g. CHRIS-PROBA, MISR) can provide additional surface properties at subpixel scale (e.g. Diner et al. 1999, 2005 Widlowski et al. 2004).

Being aware of multiple viewing angles, consider, for example, the following situation where the sensor remains pointed towards a forested ecosystem but gradually overpasses from nadir to more oblique views while taking consecutive snapshots. Then not only the observed PV and NPV proportions might change per image but also, depending on forward scatter or backscatter observations, the PV and NPV spectra are equally subject to change (e.g. predominantly shaded conditions vs. predominantly sunlit conditions).

EMs are usually obtained from spectral libraries or from the images themselves (e.g. Ichoku and Karnieli 1996). Regarding the BRDF effects, extracting EMs from each angular scene would be the most adequate but it is impossible to encounter pure pixels in a forested scene (e.g. NPV). To bypass this limitation in this study, a radiative transfer model was used that

\* Corresponding author

realistically describes the physics of canopy reflectance based on abstraction of the canopy. With such a model the reflectance of a purely vegetated canopy (PV) and a purely woody canopy (NPV) can be reasonably simulated. Modelled PV and NPV reflectance trends both in the spectral and angular domain, expressed by the bidirectional reflectance factor (BRF), were proposed to act as EMs. The hybrid 3-D radiative transfer/geometric Forest Light (FLIGHT) canopy model based on Monte Carlo simulation of photon transport (North 1996) was used for this purpose.

The objective of this study is: (1) to assess how fractional coverage of PV or NPV responds to changing viewing angles by using linear unmixing, and: (2) how such effects are related to single reflectance bands and vegetation indices. In forest canopies, woody material plays a small but significant role in determining reflectance, especially those with leaf area index (LAI) <5.0 (Asner 1998). However, the author advocated that this is also dependent on the location of woody material within the canopy.

This study is focused on coniferous forests where the woody material (stem) is well separated from the vegetated crown. We hypothesize therefore that at greater viewing angles a greater proportion of NPV in the reflectance signal will become apparent due to a greater contribution of woody stems. This is especially probable in sparse coniferous stands and when observed in backscatter direction where the influence of shadowing is reduced.

## 2. METHODOLOGY

We address two approaches to test the above hypothesis: (1) a modelling exercise that mixes the pure BRFs into various canopy reflectances and (2), a linear unmixing exercise that uses five consecutive Compact Higher Resolution Imaging Spectrometry (CHRIS) images from five different viewing angles during a single overpass of an alpine forested ecosystem (hereafter, referred to as *angular unmixing*). In an earlier study using CHRIS (Verrelst et al. 2007) it appeared that vegetation indices shows a pronounced anisotropic behaviour, especially the light use efficiency indices. It was suggested that an eventual increased proportion of woody material could significantly affect those photosynthetic-sensitive VIs. The modelling exercise will validate this assumption by mimicking each VI with increasing NPV proportions at greater viewing angles, while the angular unmixing exercise will verify whether this assumption holds true when using the original CHRIS data.

### 2.1 Data and study site

CHRIS mounted onto Project for On-board Autonomy (PROBA) offers ideal opportunities to assess the effects of changing composite proportions over varying angles. Its specifications are shown in table 1. The used CHRIS image set, acquired on June 27 2004 10:41h AM local time under partly cloudy conditions (1/8<sup>th</sup> cloud cover) was geometrically and radiometrically corrected following an approach dedicated for rugged terrains (Kneubühler et al. 2005). The test site has a geometric accuracy for the five scenes of 1-2 pixels. The generated 'surface reflectance' represents hemispherical-directional reflectance factor (HDRF) (Schaeppman-Strub et al. 2006). Due to the cloud contamination the +55° scene was discarded in further analysis. The +21° scene is the (near-) nadir scene while the -55° scene happened to be viewing predominantly back scattering (figure 1).

Sampling	Image area	Spectral bands	Spectral range
~17 m @ 556 km altitude	13 x 13 km (744 x 748 pixels)	18 bands with 6-33nm width	447-1035 nm

Table 1. CHRIS configurations for Land Mode 3

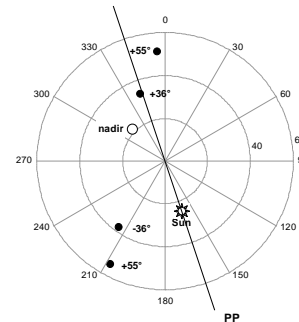


Figure 1. Polar plot of CHRIS acquisition and illumination geometry as of June 27, 2004. PP: principal plane

The study site is located in the eastern Ofenpass valley, which is part of the Swiss National Park (SNP) in South East Switzerland (10°13'48"E/46°39'45"N). The Ofenpass represents a dry inner-alpine valley with rather limited precipitation (900-1100 mm/a) on an average altitude of about 1900 m a.s.l. The south-facing slope of the Ofenpass valley is considered as the core test site. The relatively flat part down-hill (slope < 10°), which consists of old-growth coniferous forest and an alpine meadow, were chosen as study site to assess angular PV and NPV proportions.

The evergreen coniferous forest is dominated by mountain pine (*Pinus Montana ssp. arborea*). The forest is characterized by varying density and a relatively high woody fraction (ca. 30%) due to the advanced age of the pine forest and nature management practice that stopped 70 years ago. Average LAI is 2.2 (1.0 SD). The forest ecosystem can be classified as woodland associations of *Erico-Pinetum mugo*. The understorey is characterized by low and dense vegetation composed mainly of *Vaccinium*, *Ericaceae*, and *Seslaria* species

### 2.2 FLIGHT modelling

With FLIGHT, evaluation of BRF is achieved by ray tracing the photon trajectory within the discontinuous environment of a simulated forest canopy. The model allows the representation of complex vegetation structures and a correct treatment of spectral mixing resulting from multiple scattering within the scene. FLIGHT simulates a 3D forest canopy by geometric primitives with defined shapes and positions of individual stands with associated shadow effects. Within each crown envelope foliage is approximated by volume-averaged parameters with optical properties of both leaf and woody scattering elements (North 1996).

We simulated canopy reflectance of an exclusive PV and an exclusive NPV forest scene as a function of canopy variables and CHRIS acquisition geometries. The main difference between the PV and NPV simulations are that in the PV case each crown envelope (cone) represents 100% foliage, while in the NPV case each cone represents 100% bark. As input for FLIGHT averaged field measurements were used based on surveys in 4 core test sites within the forest (see table 2). The foliage optical properties were modelled by PROSPECT and coupled with FLIGHT (Kötz et al. 2004) while the spectral properties of the woody parts and background were characterized by spectrometric field measurements. Since

background is equally a mixture of PV and NPV signals (e.g. shrubs, litter) alternatively we also modelled an ‘extreme’ PV scene with background consisting of purely foliage reflectance and an ‘extreme’ NPV scene with background consisting of purely bark reflectance (see figure 2). The resultant BRF’s will act as synthetic endmembers.

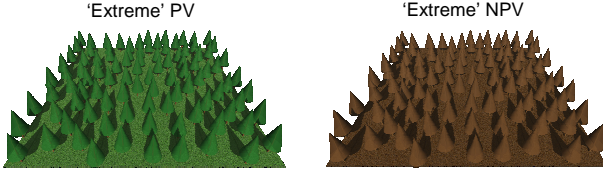


Figure 2: Visualization of a rendered purely PV canopy and a purely NPV canopy

The generated BRF’s will also be used to realize the inverse of linear unmixing. By mixing both modelled spectra in various mixtures at varying viewing angles, more natural forest canopy reflectances can be simulated. Having then PV and NPV proportions controlled, finally the angular response of vegetation indices can be assessed.

Prior to such mixing, we tested whether this straightforward approach does not conflict with the basic physical assumption of linear unmixing. This assumption states that there is not a significant amount of photon multiple scattering between macroscopic materials, in such a way that the flux received by the sensor represents a summation of the fluxes from the cover types and the fraction of each one is proportional to its covered area (Camacho-De Coca 2004). However, when photons interact with vegetation components in vertical space reflectance has the potential of becoming nonlinear (Myneni et al. 1989, Borel and Gerstl 1994). The complex FLIGHT model is specifically designed to trace these scattering trajectories depending on how each macroscopic or foliage microstructure is defined. But with the PV-NPV approach, a second problem arose due to the different nature of both constituents. A crown of 100% PV foliage propagates photons and causes further within-crown multiple scattering whereas a crown built of 100% opaque NPV foliage inhibits any further transmittance.

We compared therefore for two wavelengths ( $R_{531}$  and  $R_{570}$ ) how (post-modelling) mixed BRF signals differed with the resulted BRFs of simulated likewise mixed (pre-modelling) PV-NPV crown envelopes, while keeping the other parameters constant. As outcome of this small exercise it appeared that the BRF mixtures were conform with the BRFs of the simulated mixed PV-NPV crown envelopes (RMSE: 0.022, no significant difference found with a student’s *t*-test). This justifies the approach of post-modelling PV-NPV mixtures without having to rerun the radiative transfer code. Nevertheless, it has to be tested whether this apparent linearity is also valid for other wavelengths.

Name	Value/ Range	PV	NPV
Fractional cover (%)	0.64		
Leaf Area Index	2.4		
Fraction of green foliage (%)		100%	0%
Fraction of bark (%)		0%	100%
Soil		Vegetation	bark
Incident zenith ( $^{\circ}$ ), $\theta_i$	24.0		
Reflected zenith ( $^{\circ}$ ), $\theta_r$	-54.6, -37.8, +21.2 (nadir), +33.3, +51.1		

Table 2. Averaged input variables for FLIGHT based on surveys at 4 test sites. (Remaining input variables are described in Kötz et al. 2004)

### 3. RESULTS AND DISCUSSION

#### 3.1 Comparison VIs: FLIGHT vs CHRIS

Figures 3a and 3c show the angular shapes of the Structure Invariant Pigment Index [SIPI:  $(R_{800} - R_{455}) / (R_{800} + R_{705})$ ] and the Anthocyanin Reflectance Index [ARI:  $(R_{550})^{-1} - (R_{700})^{-1}$ ] that were calculated from CHRIS forest HDRFs. Figure 3b and 3d show the same indices calculated from the modelled BRFs according to the sun/view geometry of CHRIS. These graphs encompass various mixtures of PV and NPV proportions (%NPV= 100-%PV) with increasing NPV values at greater angles. The outer lines are the extremes: the VI response for the exclusively simulated PV forest (blue line), and the VI response for the exclusively simulated NPV forest (pink line). To facilitate comparison each index was normalized against its nadir value, or in case of the simulations, the nadir value of 100% PV.

The modelling examples confirmed earlier observations that while some indices are extremely sensitive to viewing angles, other indices respond rather invariant (Verrelst et al. 2007). In turn, it also confirmed the hypothesis that the magnitude of NPV proportion in the signal governs the VI response. By varying the proportions of NPV at greater viewing angles, a shape was attained which is likewise to that for the VIs calculated by CHRIS. Regarding other VIs the same trend was noted (not shown here), although some VIs matched better than others (for a list of the VIs and formulas see table 3). In conclusion, these examples provided a firm basis that increased NPV at greater viewing angles exert influence on the VI response.

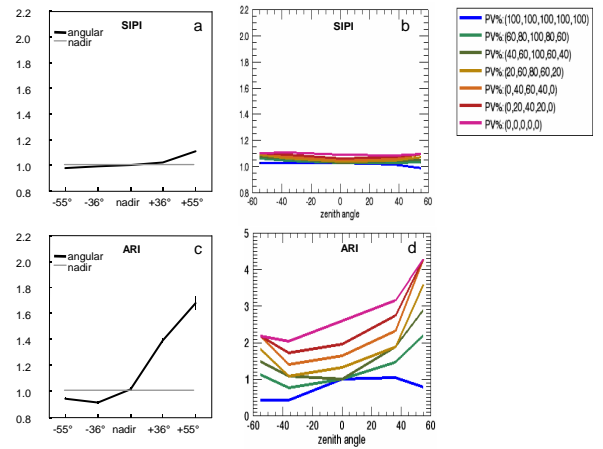


Figure 3. Averaged angular VIs (SIPI, ARI) from forest acquired by CHRIS (a, c). VIs derived from combined FLIGHT-BRFs with varying proportions of PV and NPV along the CHRIS viewing geometry (b, d). (%NPV=100-%PV)

#### 3.2 Constrained angular unmixing of CHRIS data

The second part of the study enclosed the angular spectral unmixing. Thereby, the unmixing was forced to be fully constrained (Eq. 2). This guaranteed a physical interpretation of the results since the fractions sum up to 100% and all the fractions are positive. Linear spectral unmixing provided two main outputs: the sub-pixel fractional land cover composition itself and the spectral root mean square error (RMSE) per pixel. The RMSE was used to analyze the performance of the spectral unmixing when removing bands (Zurita-Milla et al. 2007). CHRIS bands 1 and 2 (centered around 442 and 490 nm) were

omitted, as they are very susceptible to aerosol scattering. Bands 17 and the last band (centered around 905 and 1019 nm) were also excluded because these coincide with the absorption features of oxygen and water vapour; thus not adding relevant information to forest cover interpretation. The removal of these bands resulted in a RMSE of less than 5%.

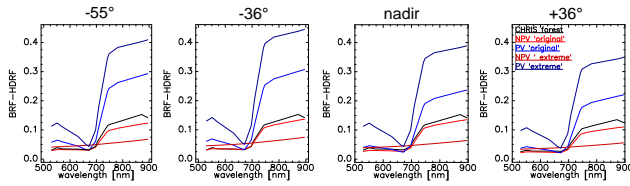


Figure 4. Angular endmembers (BRFs), plus a signature of an average forest canopy at CHRIS acquisition geometries.

Figure 4 shows a typical forest canopy reflectance of the 4 angular scenes plus the retrieved EMs. In general, CHRIS reflectance appeared to be considerably lower than the EMs. This is especially notable for the ‘original’ (background from spectrometric field measurements) NPV-EM that appears to be similar to an average CHRIS forest signature. Here, the rather vegetated background spectra dominated the canopy reflectance of the simulated NPV scene. Consequently the NPV fractions were overestimated. To correct for this, alternative ‘extreme’ scenes were simulated to ensure that the background was pure in both cases. In spite of these adjustments, however, NPV overestimation remained.

Apart from nonlinearity, the impression arose that endmember uncertainty is playing a crucial role when applying modelled EMs in satellite data unmixing. Reasons of EM uncertainty are: (1) variability in spectrometric field measurements, (2) variability in model parameters, (3) model simplifications, and (4) mismatch between BRDF (FLIGHT) and HDRF (CHRIS).

Although endmember uncertainty inhibits reliable measures, yet with BRDF-adapted EMs it is assumed that the degree of error will be the same for all angular scenes. Subsequently, the *quantity of change* from one unmixed angular scene towards another unmixed scene is considered as a more reliable measure. More appealing therefore is to compare the effect of NPV change ( $\Delta$ NPV) to change in a single waveband ( $\Delta$ HDRF<sub>w</sub>) or a derived VI ( $\Delta$ VI). Change is defined as the normalized % difference of  $-55^\circ$  value compared to the nadir value. E.g. for  $\Delta$ NPV:

$$\Delta\text{NPV} = \frac{\text{NPV}_{-55^\circ} - \text{NPV}_{\text{nadir}}}{\text{NPV}_{\text{nadir}}} * 100\% . \quad (4)$$

Figure 5 shows two examples of scatter plots where the normalized  $\Delta$ NPV is plotted against the normalized  $\Delta$ HDRF (of the wavebands 570 nm and 748 nm). Pixels plotted along the positive x-axis represent an increase in observed NPV, while negative values along the x-axis represent a decrease of observed NPV and thus an increase in PV. The square Pearson correlation coefficients  $r^2$  are shown in the graphs. Following, for each waveband a linear regression and correlation coefficient with  $\Delta$ NPV was calculated and then plotted (figure 6). The unmixing with the ‘extreme’ EMs resulted in higher correlations. Particularly in the NIR wavelengths high  $r^2$ s were reached. In the NIR domain, scattering is very high and constitutes the main source of radiation flow with maximal interactions, such that an angular change in canopy composition will lead to a pronounced change in angular outflow.

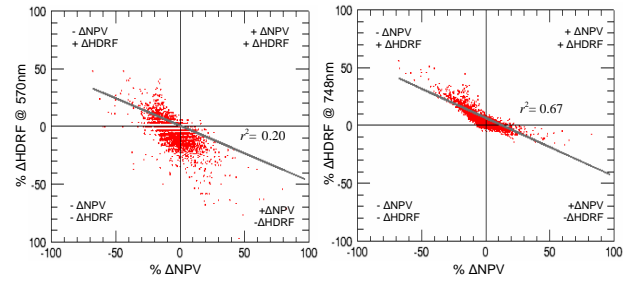


Figure 5. Scatter plots of %  $\Delta$ NPV compared to %  $\Delta$ HDF for waveband 570 nm and 748 nm

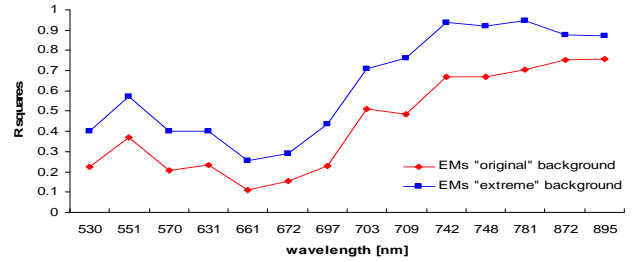


Figure 6. The  $r^2$ 's of the linear regression when correlating  $\Delta$ NPV with  $\Delta$ HDF

Linear regression relationships were in table 3 in an analogous way calculated for scatter plots of  $\Delta$ NPV against a suite of VIs ( $\Delta$ VI). Correlations were weak when considering the complete data set ( $r^2_{\text{max}}=0.21$ ). When splitting the data set into (i) pixels where a PV increase occurred (more vegetation observed at  $-55^\circ$ ), and (ii) pixels where a NPV increase occurred (more woody parts observed at  $-55^\circ$ ), then better correlations revealed (table 3). Poor correlations were found in case of the increasing PV proportions ( $r^2_{\text{max}}=0.10$ ). Yet, in case of increasing NPV proportions remarkably higher correlations were yielded. In the latter, apart from PRI and RGRI, NPV differences captured about one third of the VI variance ( $r^2$ 's between 0.24 and 0.47).

NPV effects significantly affected the reflectance signal, though since validation data is absent, results ought to be interpreted with care. Nonlinearity and EM uncertainty are undermining the applied angular unmixing approach. Generating EMs by means of forward radiative transfer modeling is advantageous with respect to controlling BRDF variables, but it also has its limitations. For instance FLIGHT does not account for within-shoot scattering, which causes the low NIR reflectance in coniferous areas (Rautiainen & Stenberg 2005). Also, understory vegetation, which can be very abundant and variable and can considerably influence the reflected signal of the stand (Rautiainen 2005), was simply generalized in this study.

To reduce EM uncertainty, rather than relying on one generalized set of EMs, further research would be through the generation of EM sets that cover a range of spectral variability according to the satellite data (Asner & Lobell 2000). Embedding a set of PV and NPV endmembers in the unmixing procedure will lead to a set of PV and NPV fractions which can afterwards be aggregated again to single PV and NPV fractions. Another approach worthwhile to explore is to apply a so-called ‘spatial unmixing’. In spatial unmixing the EMs are selected on a high resolution image while, by means of fusion, the spectral resolution is obtained from the original low resolution image (Zurita-Milla et al., 2006). This technique could solve the EM uncertainty for the image with the same geometry conditions (e.g. nadir), but does not apply to other viewing angles due to the aforementioned BRDF effects. Combining spatial unmixing

Index	Formula	$r^2$			
		+ %PV 'original'	+ %PV 'extreme'	+ %NPV 'original'	+ %NPV 'extreme'
NDVI	$(R_{\text{NIR}} - R_{\text{RED}})/(R_{\text{NIR}} + R_{\text{RED}})$	0.00	0.00	0.42	0.45
SRI	$R_{\text{NIR}}/R_{\text{RED}}$	0.03	0.03	0.39	0.39
ARVI	$(R_{\text{NIR}} - (2R_{\text{RED}} - R_{\text{BLUE}})) / (R_{\text{NIR}} + (2R_{\text{RED}} - R_{\text{BLUE}}))$	0.02	0.02	0.39	0.45
NDVI <sub>705</sub>	$(R_{750} - R_{705}) / (R_{750} + R_{705})$	0.00	0.00	0.27	0.24
mSRI <sub>705</sub>	$(R_{750} - R_{445}) / (R_{705} + R_{445})$	0.03	0.04	0.19	0.24
mNDVI <sub>705</sub>	$(R_{750} - R_{705}) / (R_{750} + R_{705} - R_{445})$	0.03	0.04	0.20	0.25
PRI	$(R_{531} - R_{570}) / (R_{531} + R_{570})$	0.01	0.00	0.00	0.01
SIPI	$(R_{800} - R_{455}) / (R_{800} + R_{705})$	0.05	0.06	0.25	0.32
RGRI	Mean of all bands in the red range divided by the mean of all bands in the green range	0.01	0.00	0.03	0.03
ARI	$(R_{550})^{-1} - (R_{700})^{-1}$	0.10	0.08	0.43	0.47

Table 3. Definition of VIs evaluated and  $r^2$ 's of selected VIs when separating the data pool in +%PV and +%NPV

with a model-generated BRF variability to correct for the angular images will be tackled in a follow-up study.

### 3.3 Normalized Difference NPV Index

Finally, having recognized that canopy structural variability can be assessed when combining multiple view angles, the next step is to develop a forest structure index. Several indices that combine multiple viewing angles already exist, such as the anisotropy index (ANIX), that is defined as the ratio of the maximum and minimum BRF (Sandmeier et al. 1998), or the normalized difference angular index (NDVAI), that uses a combination of forward and backward scattered radiation (Nolin et al. 2002). These indices are proxies for surface roughness; they indicate the degree of anisotropy but do not quantify angular land cover variability. Here, we intend to go one step further by developing a forest structural proxy that makes use of derived directional fractions rather than of directional reflectance. We define the Normalized Difference NPV Index (NDNPVI) as follows:

$$NDNPVI = \frac{NPV_{\text{back}} - NPV_{\text{nadir}}}{NPV_{\text{back}} + NPV_{\text{nadir}}}, \quad (5)$$

where 'back' corresponds to the fractions at the  $-55^\circ$  viewing angle. Note that using PV fractions in the equation would equally hold true, but since our interest was specifically to assess the angular variability of NPV we felt the above formulation being more appropriate. The NDNPVI is calculated for the study site (figure 7).

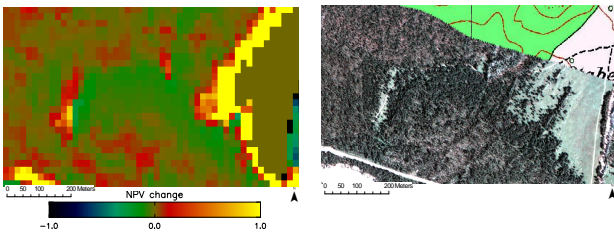


Figure 7. left: the NDNPVI; right ROSIS image (RGB) of the study site on top of the topographic map.

The green-brownish colour indicates that at those areas no angular fractional change took place, which accounts for the largest part of the study site. Areas with a more greenish colour indicate a greater fraction of observed PV at  $-55^\circ$ , whereas areas with a more reddish colour indicate a greater angular fraction of observed NPV at  $-55^\circ$ .

Where the boundary between forest and another land cover without NPV (e.g. meadow) occurs, however, the NDNPVI loses its sensitivity. The broad yellow strip north-west of the meadow is the result of no NPV fractions observed at nadir (exclusive meadow cover) while observing NPV fractions in backscatter direction. Having then zeros for  $NPV_{\text{nadir}}$  in both the numerator and denominator will always result one, whatever the NPV fractions of  $NPV_{\text{back}}$  are. Within the forest, the NDNPVI is well able to map angular fractional variability; in this way it distinguishes fully vegetated areas from woody areas. The NDNPVI can function as a suitable proxy to provide more insight in per-pixel structural canopy composition. This knowledge is crucial when attempting to interpret spectral-derived products, especially in case of photosynthesis-sensitive indices where NPV is a serious confounding factor.

## 4. CONCLUSION

The objective of this study was to assess how fractional coverage of PV or NPV responds to changing viewing angles and thereby how such effects are related to single reflectance bands and VIs. With FLIGHT the reflectance of an exclusively PV and an exclusively NPV forest scene were simulated as a function of coniferous forest variables and CHRIS acquisition viewing geometries. We used two approaches (1) a modeling exercise where VIs were calculated from controlled PV and NPV canopy mixtures, and (2) a linear unmixing exercise where PV and NPV proportions were extracted from angular CHRIS images and then correlated with the derived VIs. The modeling exercise showed that varying the NPV proportions at greater zenith angles did indeed govern the angular shape of VIs. The unmixing approach, however, was facing limitations in extracting reliable absolute fractions from the images themselves. Therefore the relative measure of  $\Delta NPV$  rather than the absolute measure was considered being more reliable. When restricting to only those pixels where the NPV proportions increased (from nadir to backscatter) then moderate correlations were obtained with the angular variability of VIs. Alternative canopy variables that were not, or not well, mimicked by the modeled EMs in combination with limitations of the explored approach made that only a small part of the VIs' angular variability was explained by the EMs. Finally, a volumetric canopy composition proxy was developed that capitalizes on the derived angular fractions. In the context of canopy photosynthesis studies, information about the canopy composition is crucial, though the work is still in an initial stage. Further efforts should be devoted to the robustness of this proxy and to the operability of the unmixing procedure.

## 5. ACKNOWLEDGEMENT

S. Schaminee is thanked for generating the visualisations of the PV and NPV forest. The work of J. Verrelst was supported through the Dutch SRON GO programme (Grant-No. EO-080).

## 6. REFERENCES

- Adams, J. B., Sabol, D. E., Kapos, V., Filho, R. A., Roberts, D. A., Smith, M. O., et al. 1995. Classification of multispectral images based on fractions of endmembers: Application to land-cover change in the Brazilian Amazon. *Remote Sensing of Environment*, 52(2), pp. 137-154.
- Asner, G. P. 1998. Biophysical and biochemical sources of variability in canopy reflectance. *Remote Sensing of Environment*, 64(3), pp. 234-253.
- Asner, G. P., & Heidebrecht, K. B. 2002. Spectral unmixing of vegetation, soil and dry carbon cover in arid regions: Comparing multispectral and hyperspectral observations. *International Journal of Remote Sensing*, 23(19), pp. 3939-3958.
- Asner, G. P., & Lobell, D. B. 2000. A biogeophysical approach for automated SWIR unmixing of soils and vegetation. *Remote Sensing of Environment*, 74(1), pp. 99-112.
- Borel, C. C., & Gerstl, S. A. W. 1994. Nonlinear spectral mixing models for vegetative and soil surfaces. *Remote Sensing of Environment*, 47(3), pp. 403-416.
- Camacho-De Coca, F., Garcia-Haro, F. J., Gilabert, M. A., & Melia, J. (2004). Vegetation cover seasonal changes assessment from TM imagery in a semi-arid landscape. *International Journal of Remote Sensing*, 25(17), pp. 3451-3476.
- DeFries, R. S., Field, C. B., Fung, I., Collatz, G. J., & Bounoua, L. 1999. Combining satellite data and biogeochemical models to estimate global effects of human-induced land cover change on carbon emissions and primary productivity. *Global Biogeochemical Cycles*, 13(3), pp. 803-815.
- Diner, D. J., Asner, G. P., Davies, R., Knyazikhin, Y., Muller, J. P., Nolin, A. W., et al. 1999. New Directions in Earth Observing: Scientific Applications of Multiangle Remote Sensing. *Bulletin of the American Meteorological Society*, 80(11), pp. 2209-2228.
- Diner, D. J., Braswell, B. H., Davies, R., Gobron, N., Hu, J., Jin, Y., et al. 2005. The value of multiangle measurements for retrieving structurally and radiatively consistent properties of clouds, aerosols, and surfaces. *Remote Sensing of Environment*, 97(4), pp. 495-518.
- Ichoku, C., & Karnieli, A. 1996. A Review of Mixture Modeling Techniques for Sub-Pixel Land Cover Estimation. *Remote Sensing Reviews*, 13(3-4), pp. 161-186.
- Kneubühler, M., Koetz, B., Itten, K., Richter, R., & Schaepman, M. 2005. *Geometric and radiometric pre-processing of CHRIS/PROBA data over mountainous terrain*. European Space Agency, (Special Publication) ESA
- Kötz, B., Morsdorf, F., Itten, K., Schaepman, M., Bowyer, P., & Allgöwer, B. 2004. Radiative transfer modeling within a heterogeneous canopy for estimation of forest fire fuel properties. *Remote Sensing of Environment*, 92(3), pp. 332-344.
- Myneni, R. B., Ross, J., & Asrar, G. 1989. A review of the theory of photon transport in leaf canopies. *Agricultural & Forest Meteorology*, 45(1-2), pp. 1-153.
- Nolin, A. W., Fetterer, F. M., & Scambos, T. A. 2002. Surface roughness characterizations of sea ice and ice sheets: Case studies with MISR data. *IEEE Transactions on Geoscience and Remote Sensing*, 40(7), pp. 1605-1615.
- North, P. R. J. 1996. Three-dimensional forest light interaction model using a monte carlo method. *IEEE Transactions on Geoscience and Remote Sensing*, 34(4), pp. 946-956.
- Rautiainen, M. 2005. Retrieval of leaf area index for a coniferous forest by inverting a forest reflectance model. *Remote Sensing of Environment*, 99(3), pp. 295-303.
- Rautiainen, M., & Stenberg, P. (2005). Application of photon recollision probability in coniferous canopy reflectance simulations. *Remote Sensing of Environment*, 96(1), pp. 98-107.
- Roberts, D. A., Smith, M. O., & Adams, J. B. 1999. Green vegetation, nonphotosynthetic vegetation, and soils in AVIRIS data. *Remote Sensing of Environment*, 44(2-3), pp. 255-269.
- Sandmeier, S., Muller, C., Hosgood, B., & Andreoli, G. 1998. Physical mechanisms in hyperspectral BRDF data of grass and watercress. *Remote Sensing of Environment*, 66(2), pp. 222-233.
- Schaepman-Strub, G., Schaepman, M. E., Painter, T. H., Dangel, S., & Martonchik, J. V. 2006. Reflectance quantities in optical remote sensing--definitions and case studies. *Remote Sensing of Environment*, 103(1), pp. 27-42.
- Settle, J. J., & Drake, N. A. 1993. Linear mixing and the estimation of ground cover proportions. *International Journal of Remote Sensing*, 14(6), 1159-1177.
- Van Leeuwen, W. J. D., & Huete, A. R. 1996. Effects of standing litter on the biophysical interpretation of plant canopies with spectral indices. *Remote Sensing of Environment*, 55(2), pp. 123-138.
- Verrelst, J., Schaepman, M.E., Koetz, B., & Kneubühler, M. 2007. Angular sensitivity of vegetation indices derived from CHRIS/PROBA data in two Alpine ecosystems. *Remote Sensing of Environment*. (in revision)
- Widlowski, J. L., Pinty, B., Gobron, N., Verstraete, M. M., Diner, D. J., & Davis, A. B. 2004. Canopy structure parameters derived from multi-angular remote sensing data for terrestrial carbon studies. *Climatic Change*, 67(2-3), pp. 403-415.
- Zurita-Milla, R., Clevers, J. G. P. W. & Schaepman, M. 2006. LANDSAT TM and MERIS FR image fusion for land cover mapping over the Netherlands. *2nd Workshop of the EARSeL SIG on Land Use and Land Cover*. Bonn, Germany.
- Zurita-Milla, R., Clevers, J. G. P. W., Schaepman, M. E. & Kneubühler, M. 2007. Effects of MERIS L1b radiometric calibration on regional land cover mapping and land products. *International Journal of Remote Sensing*, 28, pp. 653-673.